Modeling for Preliminary Stray Current Design Assessments: The Effect of Crosstrack Regeneration Supply

Charalambos A. Charalambous, *Member, IEEE*, Ian Cotton, *Senior Member, IEEE*, and Pete Aylott

***Abstract*—Simulators of different approaches and scales have been reported in the literature in an attempt to investigate the generation and impact of stray currents resulting from the operation of dc rail transit systems. Bearing in mind the existing methods for stray current modeling and control, this paper offers an important modeling advancement. A model is developed to quantitatively assess the more complex stray current picture arising from the effect of crosstrack regeneration supply. Crosstrack regeneration refers to the case where a train in one tunnel is collecting current from a regenerating train in an adjacent tunnel, as a power-saving endeavor.**

***Index Terms*—Bored tunnel systems (BTS), corrosion risk, crosstrack regeneration, dc transit systems, stray current design and control.**

I. Introduction

THE ELEVATION in rail potential caused by the flow of traction current has the ability to cause current leakage from the rails, usually described as stray current. Corrosion will occur at each point that current transfers from a metallic conductor, such as a reinforcement bar in concrete, to the electrolyte (i.e., the concrete). Hence, stray current leakage can cause corrosion damage to the rails, the tunnel reinforcement, and to third-party systems, such as external buried pipework. Severe damage may occur as a result of stray current leakage [1].

The stray current impact of any individual dc railway can be managed in a number of ways. In broad terms, the issues that impact stray current performance can be summarized as: 1) the conductivity of the traction current return circuit (i.e., the rails); 2) the quality of insulation of the return circuit from earth; 3) spacing of supply substations; 4) train current demand; 5) substation and system earthing; and 6) regenerative braking.

A thorough literature review reveals that the majority of the constraints listed are well defined and understood. In particular, the impact on stray current levels due to conductivity and insulation of the return circuit is reported in [2]–[5]. Other related literature describes the influence of train current demand on the dc traction stray current perfomance, both statically and dynamically [6]–[10]. Moreover, the different substations and system earthing schemes utilized in dc traction systems and their influence in their stray current performance are addressed in [11] and [12].

However, it appears that there is a gap in the literature regarding simulation models that are able to quantitavely assess the stray current performance of dc traction systems under the effect of crosstrack regeneration. Under this condition, the stray current distribution of the system becomes more complex.

A. Crosstrack Regeneration and Stray Current Performance Evaluation

Crosstrack regeneration refers to the case where a train on one set of running rails is collecting current from a regenerating train on an adjacent set of running rails as a power-saving endeavor. A comprehensive description of dc-traction power system software that enables the situation, with trains operating in regenerative-braking mode, to be simulated is reported in [13].

In the context of stray current assessments for dc traction systems, the stray currents produced during regenerative braking operation are not thought to be adequately controlled. However, the effect of crosstrack regeneration has not been quantitatively assessed in the literature. A recent work [14] merely reports that the introduction of regenerative braking has had a significant (negative) impact on the capability to safely mitigate dc stray currents. This is because regenerative braking converts the dc traction locomotive into a moving power source during braking operations; therefore, the source and load move around the system, making it difficult to design an effective stray current mitigation system. As a result, many stray current modeling endeavors report that the effect of regenerative braking is inevitably ignored at the early stage of the stray current control design process [15], [16].

Consequently, the main objective of this paper is to offer a quantitative assessment of the more complex stray current picture arising from the effect of crosstrack regeneration. This kind of assessment may be considered at the early stages of the design process. The models developed for this paper are based on a stray current assessment for a bored tunnel system (BTS) using a commercial software platform [17]. The design options incorporated for the static models are based on realistic 3-D civil drawings and on other particulars taken from a real system. Thus,

Manuscript received December 10, 2012; revised March 06, 2013; accepted April 19, 2013. Date of publication May 14, 2013; date of current version June 20, 2013. Paper no. TPWRD-01341-2012.

C. A. Charalambous is with the Department of Electrical and Computer Engineering, University of Cyprus, Nicosia 1687, Cyprus (e-mail: cchara@ucy.ac.cy).

I. Cotton is with the School of Electrical and Electronic Engineering, University of Manchester, Manchester, M60 1QD, U.K. (e-mail: ian.cotton@manchester.ac.uk).

P. Aylott is with Intertek- CAPCIS, Manchester M1 7DP, U.K. (e-mail: pete.aylott@intertek.com).

Color versions of one or more of the figures in this paper are available online at http://ieeexplore.ieee.org.

Digital Object Identifier 10.1109/TPWRD.2013.2259849

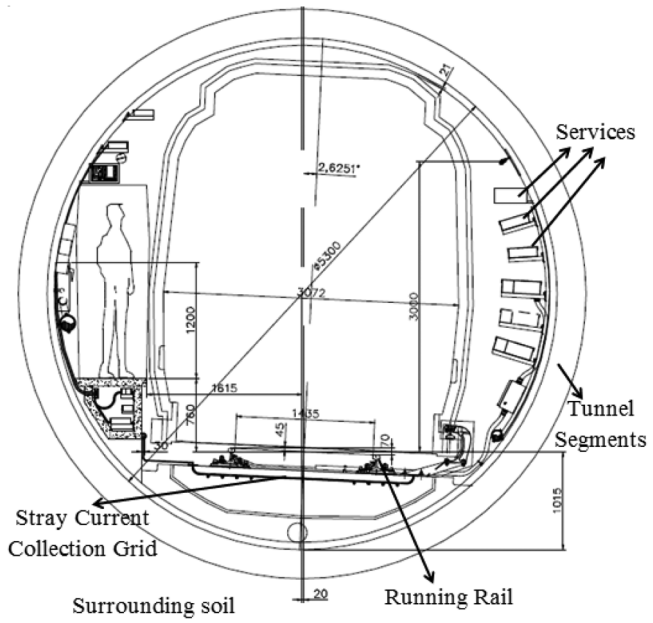

Fig. 1. Cross section of a realistic BTS with actual dimensions in millimeters.

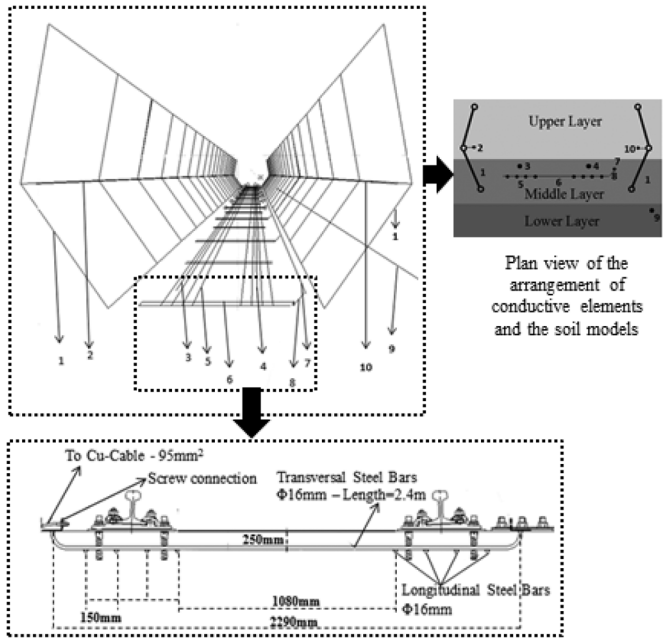

Fig. 2. Perspective view of the arrangement of conductive elements in the BTS model.

the global impact of crosstrack regeneration on the stray current collection system (SCCS), the tunnel reinforcement, and on a third-party infrastructure, can be quantitatively assessed.

II. Description of the Base Simulation Model

Fig. 1 illustrates a cross-section of a realistic BTS along with actual dimensions, labeling the most important features that are crucial in assessing its stray current performance.

A. Characteristics of the Base Simulation Model

An appropriate simulation model has been formulated within the MALZ module of the CDEGS software [17] to serve as a reference model (see Fig. 2).

The MALZ module allows currents to be injected and collected at various points in a network of conductors that are placed in a soil environment. It further computes the flow of these currents through each individual conductor within the network. It thus offers the advantage of computing a stray current and a voltage distribution along the length of the system modeled [18]. The design options are based on realistic 3-D civil drawings and on other particulars taken from a real system as shown in Fig. 2. The model embraces the return circuit elements found in a BTS. These elements are formulated by 837 individual conductors subdivided in 4793 segments. Each conductor segment is given a certain material type and coating characteristics as tabulated in Table I.

The model of Fig. 2 has also incorporated a three-layer horizontal soil model into it. For this type of soil model, the potentials are computed by using an analytically derived kernel [19]. This arrangement mirrors the real situation well and is computationally stable as detailed in [18]. The upper layer of the soil model is assigned an extremely high resistivity of $10^{14}\ \Omega\mathrm{m}$, to eliminate any leakage current to flow from the rails to tunnel services in an upward direction. A portion of the tunnel segments is situated in the middle soil layer which is assigned a resistivity of 180 Ω.m. This represents the concrete present within the tunnel. The lower layer of the soil model is assumed to have a resistivity of 15 Ωm (i.e., a lowest likely measured figure) and represents the soil surrounding the tunnel. It is reiterated that from a stray current perspective that the worst case should be the lowest likely measured soil resistivity figure and recognized that under some environmental conditions, this could be lower than the value used here. Table II tabulates the base input data and assumptions employed in subsequent simulations for assessing the stray current performance of the model in Fig. 2.

B. Description of the Energization Model-Based Scenario

The simulation model can assess the impact of a single point load at discrete locations with traction supply substations at each end. The model is also able to capture the floating nature of the system and can assess various topological design options of the BTS.

The base model assumes two cases as shown in Fig. 3. The first scenario assumes that the train is placed 500 m from the origin of the track (A), while the second scenario simulates the train at 250 m from the origin of the track (B). In both cases, the train is modeled as a motoring load (i.e., drawing 2000-A current from the two substations located at either end of the track).

It is noted that the simulated case A (i.e., symmetrical 1-km section of tunnel with a single train at the center and a substation at each end) represents the worst static case scenario in terms of stray current performance evaluation.

C. Simulation Results and Analysis

The simulations are carried out using the 1-km sections of the tunnel system illustrated by Fig. 2. The simulation takes about

TABLE I
DESCRIPTION OF CONDUCTIVE ELEMENTS

Numbered Items	Further Particulars
Tunnel Segments (Item 1)	The tunnel segments are not electrically continuous. Two segments (item 1 – left and right are considered in the model, since electrically conductive tunnel services may be attached to them. While the tunnel segments are approximately 1m in length, they are modelled as 50m segments in the computer model to restrict the overall number of conductors.
Tunnel Services (Items 2 &10)	Modelled as galvanised steel conductors. The tunnel services are modeled to represent an overall tunnel service cross-sectional area of 79 mm^2 (item 2), equating to a conductor radius of 5 mm and an overall tunnel service cross-sectional area of 314.16 mm^2 (item 10), equating to a conductor radius of 10 mm. The model allows for the tunnel services to be continuous but these are insulated from the tunnel segment reinforcement.
Running rails (Items 3 &4)	Modelled as conductors (e.g. UIC54) having a longitudinal resistance of 40 mΩ per kilometer. As it is not possible to model discrete insulator pads in the software, the effect is modeled by assuming the rails are coated with a resistive coating. This coating is set accordingly to account for a resistance to earth 100Ω.km.
Stray Current Collection Grid – Longitudinal and Transversal Steel Bars (Items 5 &6)	The S.C.C.S. consists of the Stray Current Collection Grid (S.C.C.G.) and the Stray Current Collection Cable (S.C.C.C.). The S.C.C.G. employs steel bars which are longitudinally placed (item 5) under each rail (4 steel bars x Φ16 mm for each running rail - that is 2 x 4 steel bars x Φ16 mm for a single track). This design provides an overall S.C.C.G. cross-section of 1608 mm^2 per track as is shown in Fig. 2
Stray Current Collection Copper Cable – (Items 7 & 8)	The Stray Current Collection Cable (S.C.C.C. - item 7) is bonded to the S.C.C.G. through flexible bare cables (item 8) at 100 m intervals. Both cables are made from copper and their size is taken in the model as 95 mm^2. The cables are insulated.
Third-Party Infrastructure (Item 9)	The conductor (item 9) representing the third party infrastructure serves the scope of assessing the effect of stray current on samples of the metallic infrastructure that lies in the nearby vicinity of the tunnel system. Within the model developed it takes the form of a metallic (heavy duty galvanised steel) coated conductor.

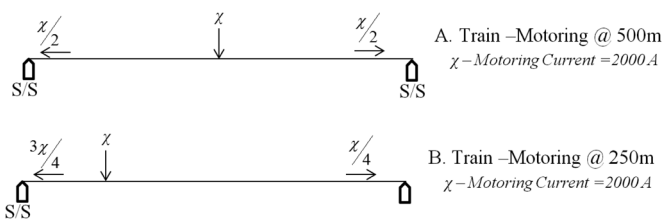

Fig. 3. Base model: One BTS with a motoring train at different locations (scenario A at 500 m—Scenario B at 250 m).

2.5 h to be completed on a standard computer (2-GHz processor, 3 GB RAM). Fig. 4 illustrates the simulated rail-to-earth voltage (for Rail_1 -item 3) simulated by the FE model of Fig. 2 for the two scenarios presented in Fig. 3. It can be shown that the same profile is obtained for Rail_2 (item 4) in each scenario. The current returns to the supply substations via the running rails; in a proportion determined by the relative location of the train with respect to its feeding substations. This produces a rise in the rail-to-earth potential which, in turn, results in stray currents in a proportion determined by the relative location of the train. In a floating rail system, the stray currents are determined by the combination of the rail potential and the resistance of the trackwork insulators.

A rough calculation of the expected stray current for scenario A can be made by hand. Take 2000 A equally by returning through a section of 500 m of two rails (i.e., 1000 A on each side) with a resistance of 40 $\mathrm{m}\Omega/\mathrm{km}$ of rail. Since the two rails are in parallel, the overall potential difference between the midpoint and rail ends will be 20 V. In the convention of this modeling, this will appear on the rails as $+10$ V to remote earth near the train and -10 V to remote earth near the two substations. A positive voltage implies a current leaking out of a conductor by corrosion; a negative voltage implies current leaking into a conductor. At 250 m down the track, the voltage to remote earth will be 0 V. The running rail is taken to have a resistance to

TABLE II
BASE INPUT DATA AND ASSUMPTIONS

Parameter (Per Tunnel/Track)	Description
Track length & power supply	1 km single track with a supply substation at either end.
Traction current	2000 A static load at 250m (motoring)
Rail resistance	40 mΩ/km (UIC54)
Rail conductance (resistance to earth)	100 Ω.km
Soil Model Resistivity /Width	Upper: 10^{14} Ω.m / 5.8m Middle: 180 Ω.m (Concrete) /1m Lower: 15 Ω.m /Infinite
Stray Current Collection Grid (S.C.C.G.)	2 x 4 steel bars x Φ16 mm for a single track
Stray Current Collector Cable (S.C.C.C)	95 mm^2 - copper – bonded to S.C.C.G. at 100m intervals
Stray current collector cable termination at substations	Floating
Tunnel Depth	6m below ground level
Tunnel Reinforcement	Φ20 mm- Steel (Tunnel segments electrically isolated along the length of tunnel)
Tunnel Services	79 mm^2 (left) / 314.16 mm^2 (right) - galvanised steel
Insulation of internal tunnel infrastructure (handrail, fire main etc.) from segment reinforcement	insulated connection to tunnel reinforcement: 1MΩ
Third Party Infrastructure	1963 mm^2 - galvanised steel

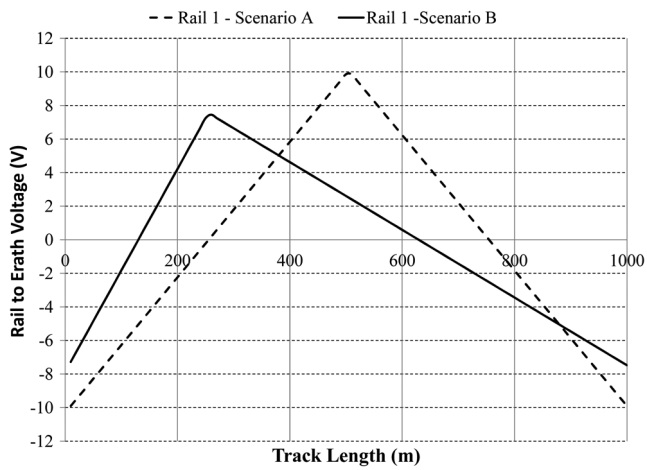

Fig. 4. Simulated track-to-earth voltage—base model.

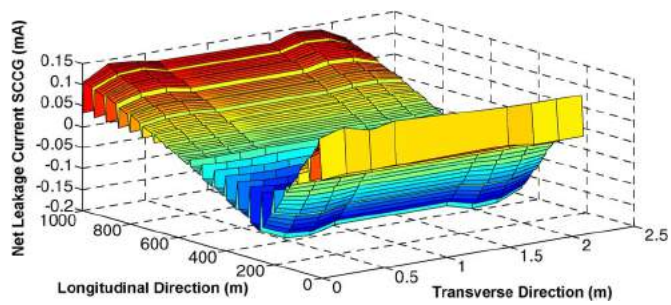

Fig. 5. Simulated net leakage current SCCG—base model—Scenario B.

earth of 100 Ωkm. The resistance to earth of 250 m of running rail is therefore 400 Ω. The total stray current leaving the running rail will therefore be given by 5 V (the average running rail voltage along a 250-m length) divided by 400 Ω, in other words 12.5 mA. The total stray current will therefore be approximately four times this, 50 mA, since there are two running rails in either of the 500-m sections which each allow current to leak to earth. A similar calculation can be shown for scenario B. Besides hand calculations, the results of Fig. 4 have been extensively verified by the classical resistive-type approach that is widely used in the literature [9], [20]. Furthermore, the software employed in this study, has itself been shown to be accurate by many researchers across the world and has been extensively verified. The models used in this paper are simplifications of a real system but these simplifications were used after confirming that they did not cause an error in any expected current/voltage of more than 1% [24].

Fig. 5 illustrates the simulated geometrically accurate 3-D plot of the net leakage current profile of the two stray current collection grids (SCCG) when the train is located 250 m from the origin (i.e., scenario B).

Fig. 6 illustrates the simulated geometrically accurate 3-D plot of the current retained by the SCCG, while Fig. 7 shows the corresponding track-to-earth voltage profile.

Table III illustrates the summary of the stray current generation and its consequent allocation simulated for the model of Fig. 2. It is noted at this point that the percentage of current flowing in the SCCS (SCCG +SCCC) (i.e., its efficiency), can be assessed at a point where the net leakage current of the SCCS is zero (see Fig. 5) and the collected current by the SCCS conductor elements is at an absolute maximum (see Fig. 6). By representing the total stray current flowing from the running rails as a percentage of the stray current collected by the grid, the efficiency of the SCCS can be determined. The remainder of the stray current will flow through unintended paths (e.g., earth).

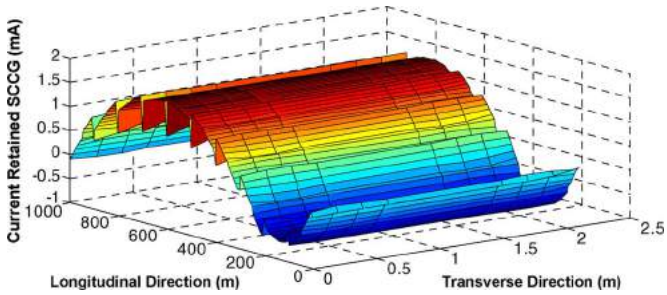

Fig. 6. Simulated retained current SCCG—base model.

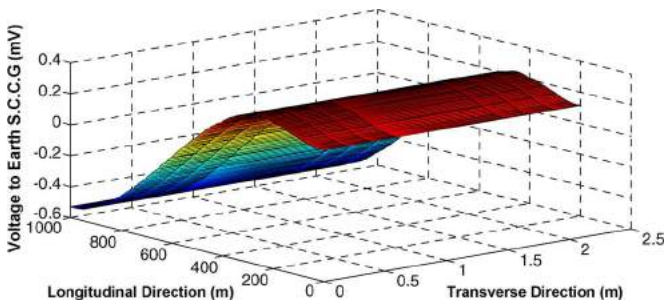

Fig. 7. Simulated track-to-earth voltage SCCG—base model.

TABLE III
SUMMARY OF RESULTS—BASE MODEL

Description	Scenario *A* Current (mA)	Scenario *B* Current (mA)
Total Stray Current Rails	50.171	37.604
Retained Current S.C.C.G.	24.983	18.328
Retained Current S.C.C.C.	17.495	12.634
Total Stray Current Tunnel Reinforcement	0.47081	0.40238
Total Stray Current Tunnel Services	0.00	0.00
Retained Current Tunnel Services	0.00	0.00
Retained Current 3rd party Infrastructure	0.2071	0.102
Efficiency of S.C.C.S	84.67 %	82.34 %
Current through unintended paths	15.33 %	17.66 %

Table III also illustrates that the total stray current calculated from the model (50.171 mA) coincides with the hand calculations (50 mA) presented earlier (Scenario *A* is in Fig. 3). As far as the total generated current is concerned, the design engineers should note that a variation in track current will influence the leakage current distribution due to the resulting alteration of rail-to-earth potential. A doubling in track current or a doubling in substation spacing (i.e., 2 km) will lead to a doubling in voltage and, hence, a resulting doubling of leakage current density along the rail. This is a linear effect.

Moreover, no current is collected by the tunnel services since these are modelled as being insulated from the tunnel reinforcement (see Table I). Finally, Fig. 8 illustrates the calculated voltage on a longitudinal axis parallel to the tunnel reinforcement (where *item 2* is attached—see Fig. 2).

It should be noted that Fig. 8 illustrates a snapshot of the simulated voltage along the specified axis. The discontinuous voltage profile confirms that the tunnel segments are electrically not continuous (i.e., the reinforcement in adjoining segments (both circumferential and longitudinal) is not in direct electrical contact as segments may be bolted together through

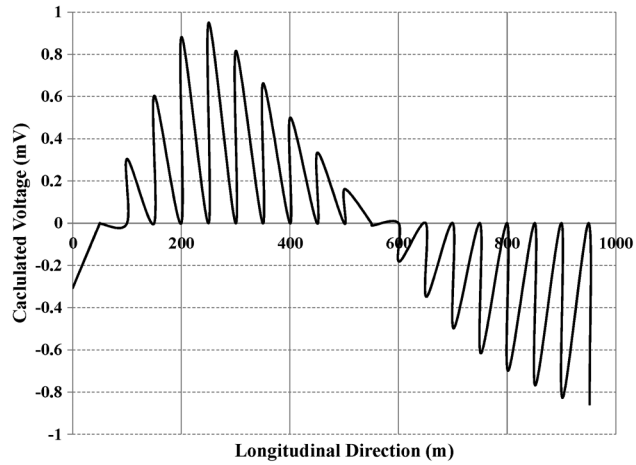

Fig. 8. Calculated voltages on a longitudinal axis of tunnel reinforcement.

PVC sleeves). This calculation may also be used as a preliminary evaluation to check whether the maximum-allowable potential value—dictated by EN 50122-2 [21] for the longitudinal voltage drop caused by operation in the tunnel is not exceeded.

III. DESCRIPTION OF CROSSTRACK REGENERATION MODEL

The developed crosstrack regeneration model is based on realistic fundamental principles of track regeneration techniques. These techniques are thoroughly described in [22] and have been integrated in a scenario where a motoring train in one tunnel is collecting current, via cross tunnel bonding of the 3rd rail supply conductor at substation and station locations, from a regenerating train in a second tunnel. It is beyond the scope of this paper to expand on the dynamics of regenerative braking in traction systems. It is reiterated that the main scope of the developed model is to quantitatively assess the more complex stray current picture arising from cross track regeneration in the circumstance where rectifiers are used to supply two tracks (i.e., trains in neighboring BTSs).

A. Characteristics of the Crosstrack Regeneration Model

Fig. 9 illustrates the 3-D geometrically accurate simulation model formulated to assess the crosstrack power (current) transfer from a regenerating to a motoring train. The same characteristics and data input assumptions tabulated in Tables I and II hold for the model of Fig. 9 as well. It is noted that both BTS (A and B) have the same design characteristics both in terms of their topological arrangement and values and are separated by a distance of 15 m.

The trains are placed 250 m from the origin of either track (i.e., there is a total train-train separation of 500 m). The train in system A (250 m) is modeled as a motoring load as in the base model Scenario B of Section I, whereas the train in system B (750 m) is modeled as a generating load.

A dc supply connection is modeled at the location of the motoring load (at 250 m). This supply connection is entitled to transfer current from the regenerating track. The connection is obviously necessary to transfer the power from one train to the other, accounting for a regeneration scenario. This is, however,

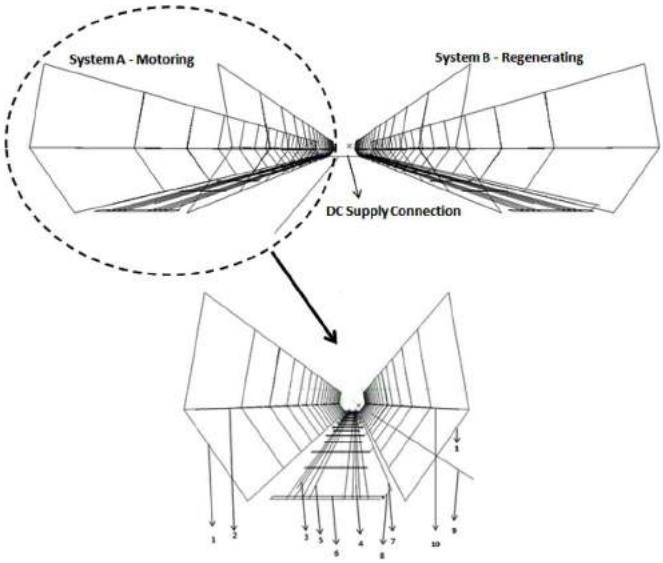

Fig. 9. Perspective view of the arrangement of conductive elements for the crosstrack regeneration model (System A—motoring at 250 m, System B—regenerating at 750 m).

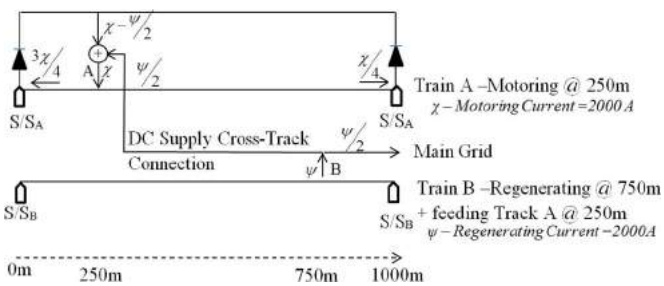

Fig. 10. Crosstrack regeneration scenario: Track A— motoring, track B—regenerating (50-50 scenario).

an artificial component of the model [17] and not a direct representation of the 3rd rail conductor circuits. It is based on current sources/sinks and cables modeled in such a way to represent a supply connection between the two tunnels (see Fig. 10).

The simulation takes about 5 h to be completed on a standard computer (2-GHz processor, 3-GB RAM).

B. Description of Energization Model (Crosstrack Regeneration)

Fig. 10 illustrates the fundamental principles of a crosstrack energisation scenario. It specifically suggests that half of the regenerated current from the train in track B (i.e., $\Psi/2 = 1000$ A) is fed to that in track A at the location of the motoring load. Therefore the motoring load is powered on a 50-50% scenario (i.e. from both systems). That is 1) by drawing current from the rectifiers that supply track A (i.e., $\chi - \Psi/2 = 1000$ A) and 2) by drawing current from the regenerating track B ($\Psi/2 = 1000$ A). Thus, a total of 2000 A (χ) is provided to the motoring load, as is the case with the scenario B of the base model described in Section II.

The modeled scenario aims to capture the case where some of the energy produced by the regenerating vehicles is used to partially supply the motoring vehicles in an adjacent tunnel. It

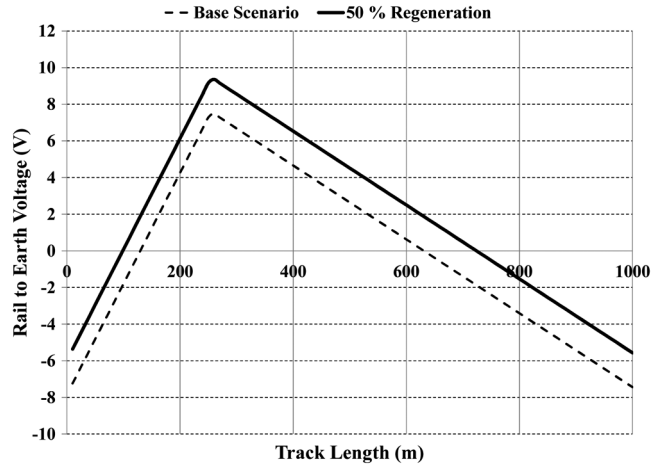

Fig. 11 Simulated track-to-earth voltage—base scenario versus 50-50 regeneration scenario.

should be noted that if the net energy produced by regenerating vehicles exceeds that used by motoring vehicles, the excess energy cannot be returned to the ac supply due to the unidirectional nature of the rectifiers (i.e., nonreceptive supply), unless appropriate control/rectifying actions are enforced; to feed the excess energy into the main power grid [22]. Therefore, the modelled scenario assumes that some regenerated power is allowed to return to the main grid supply.

C. Simulation Results and Analysis

The simulation results reflect on the effect of crosstrack regeneration supply on the motoring track A. The same effect and results are expected when the conditions are reversed (i.e., to examine the effect of crosstrack regeneration supply on track B should this become motoring). These results are benchmarked against the stray current performance of the motoring system of the base-case scenario presented in Section II. This is because in both scenarios, the motoring loads are supplied with a total of 2000 A, thus facilitating a sound comparison. Fig. 11 illustrates a comparison of the rail-to-earth voltage obtained for the motoring system of the base scenario (Section II) against the track voltage profile obtained under the crosstrack regeneration (50-50) scenario.

It is evident that the rail-to-earth potential is positively shifted by 1.875 V (although the voltage difference between the minimum and maximum voltage limits is maintained at 14 V for both cases) when the motoring load is supplied on a 50-50% scenario (i.e., 50% regeneration current from an adjacent system and 50% from its own tunnel rectifier substations). This positive voltage shift will inevitably impact on the level of the generated stray current, since the length of the track at the positive potential is increased.

Table IV illustrates the summary of the stray current generation and allocation obtained for the simulation model of Fig. 8, and benchmarks these against the results obtained for the base-case scenario (see Table III). The results confirm that crosstrack regeneration may act in reducing the efficiency of a stray current control system. More specifically, the total generated stray current has increased by 55.86% in the crosstrack regeneration

TABLE IV
SUMMARY OF RESULTS—COMPARATIVE ASSESSMENT

Description	Tunnel Current (mA) Fig. 2	Tunnel A Current (mA) Fig. 9
Total Stray Current Rails	37.604	58.99
Retained Current S.C.C.G.	18.328	19.647
Retained Current S.C.C.C.	12.634	13.237
Total Stray Current Tunnel Reinforcement	0.40238	1.043
Total Stray Current Tunnel Services	0.00	0.00
Retained Current Tunnel Services	0.00	0.00
Retained Current 3rd party Infrastructure	0.102	0.135
Efficiency of S.C.C.S	82.34 %	55.748 %
Current through unintended paths	17.66 %	44.25 %
Description	**% Change**	
Total Stray Current Rails	55.86	
Retained Current S.C.C.G.	7.09	
Retained Current S.C.C.C.	5.50	
Total Stray Current Tunnel Reinforcement	61.42	
Total Stray Current Tunnel Services	0	
Retained Current Tunnel Services	0	
Retained Current 3rd party Infrastructure	24.44%	
Efficiency of S.C.C.S	-26.59 %	

scenario. That comes despite the fact that the motoring load in track A is drawing the same current in both case scenarios (i.e., 2000 A). This is due to the positive voltage shift that the floating motoring track A experiences, as a result of being partially energized from the adjacent regenerating tunnel system.

Most importantly the ability of the SCCS of the System A to collect the generated stray current is decreased by 26.59%. It should be noted at this point, that the efficiency of the SCCS is associated with the number, size and placement of the constituent steel bars, with respect to the running rails. A further element that contributes to the efficiency of the system is the size of the stray current collection Cu cable (SCCC). The results obtained suggest that the efficiency of the SCCS can be compromised under crosstrack regeneration scenarios. This should be kept in mind during any preliminary assessments that are performed to substantiate the design specification as well as the geometric topology of the collection system.

Moreover the simulated results have indicated that is likely to experience a higher stray current flow towards the third-party infrastructure that lies in the nearby vicinity of the BTS. In this particular example, the third-party infrastructure increases its retained current by 24.44% (0.033 mA). This comes as a result of the increased stray current levels under the crosstrack regeneration scenario modeled.

Finally, Fig. 12 compares the calculated voltage on a longitudinal axis parallel to the tunnel reinforcement for the two case scenarios (crosstrack regeneration scenario and base scenario—see Fig. 8).

A maximum potential shift of 1 mV is calculated for the tunnel reinforcement under the crosstrack regeneration scenario. The calculated results could be correlated to the notes of EN 50122-2. These notes suggest that the acceptance criteria for successful control for the tunnel reinforcement potential shift are subject to a maximum limit of +0.2 V (EN50162:2004

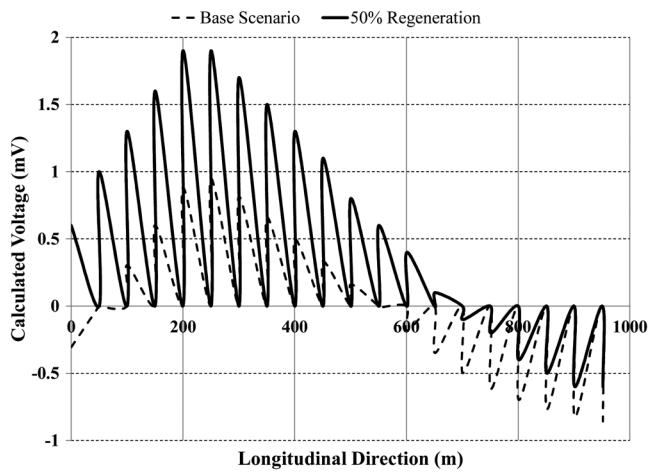

Fig. 12. Calculated voltages on a longitudinal axis of tunnel reinforcement-based scenario versus the 50-50 regeneration scenario.

Table I [23]) which EN 51022-2:2010 interprets as "the average value in the hour of highest traffic" although it should be borne in mind that the standard allows for significantly lower rail-to-earth resistance than that modeled here. It is noted that in a practical system, monitoring this voltage value, enables quantification of the stray current magnitude and direction (at the measurement location) and confirms whether a metro system is exporting and importing traction stray current through reinforced structures to and from the outside environment. This both quantifies the corrosion threat to the tunnel reinforcement and the risk of stray current corrosion to external pipes and services.

Therefore, the evaluation of the design process followed in this study has shown the means to take into account the following inputs: 1) the traction power; 2) the stray current control

TABLE V
COMPARISON UNDER DIFFERENT ENERGIZATION SCENARIOS

	Energisation Scenario			
Description	**Base**	**50-50**	**25-75**	**0-100**
Total Stray Current Rails	37.60 mA	58.99 mA	76.58 mA	150.87 mA
Retained Current S.C.C.G.	18.33 mA	19.65 mA	20.15 mA	19.23 mA
Retained Current S.C.C.C.	12.63 mA	13.24 mA	13.47 mA	12.57 mA
Total Stray Current Tunnel Services	0.00 mA	0.00 mA	0.00 mA	0.00 mA
Retained Current Tunnel Services	0.00 mA	0.00 mA	0.00 mA	0.00 mA
Retained Current 3rd party Infrastructure	0.102 mA	0.135 mA	0.160 mA	0.368 mA
Efficiency of S.C.C.S	82.34 %	55.748 %	43.90 %	21.08%
Current through unintended paths	17.66 %	44.25 %	56.1 %	78.92 %

designs as well as the distribution of the different tunnel and station construction across the system; 3) significant interfaces with third-party systems and services; and 4) crosstrack regeneration scenarios.

D. Sensitivity Analysis

A further set of simulations has been carried out to assess the influence of increasing the percentage of regeneration current that is used to energize motoring system A.

Table V tabulates a comparison of the results obtained under the 50-50 energization scenario, a 25–75 energization, and a 0–100 energization scenario. The 25–75 scenario reflects the case where the motoring load A is drawing 500 A current from the rectifiers that supply track A and, in addition, drawing 1500 A current from the regenerating track B. Thus, a total of 2000 A is supplied to the motoring load, as is the case with the base scenario. The 0–100 energization scenario reflects the case where the motoring load A draws all of its current from the regenerating track B. The latter case study assumes that the two tracks and power-supply rails are interconnected at both ends (i.e., at substations locations). The simulated results under the 0–100 scenario advocate that the impact on the proposed stray current control system will be more negatively pronounced. Table V also details that the efficiency of the SCCS is considerably decreased when benchmarked against the efficiency obtained for the base scenario. Moreover, the negative impact on the third-party infrastructure is more pronounced under the 0–100 energization scenario.

On a final note, Fig. 13 provides the means to interpret the tabulated results of Table V. It is shown that the leakage stray current density profiles are altered for each scenario modeled although the train is supplied by the same load current (i.e., 2000 A). A positive stray current density in Fig. 12 represents the case where a current leaks out of the rails into the environment. For the negative stray current density case, the current leaks back to the rails. Therefore, the simulated stray current profile of the 0–100 energization scenario suggests

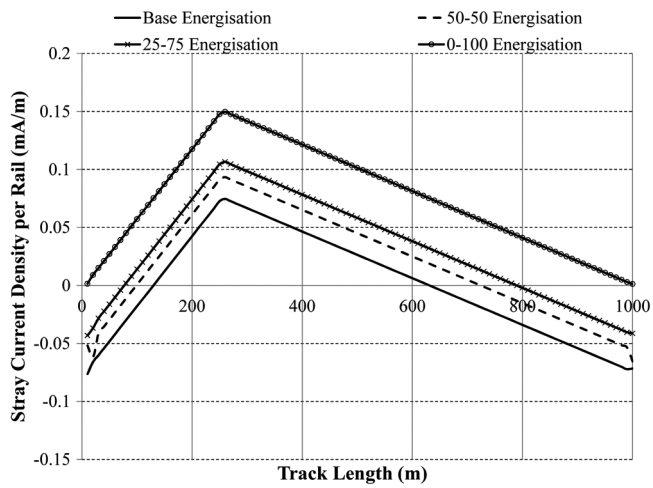

Fig. 13. Comparison of stray current densities per rail under different scenarios.

that more corrosive stray current is to leave the rails since the rail region with a positive current density is increased when compared to the other cases modeled. The magnitude of the current leaking from the rails is determined by the voltage to remote earth at any point along the track and the resistance to remote earth of each rail.

E. Proposed Mitigation Measures

Cross bonding the rails/tracks might be one option for the design engineers to reduce the stray current generation and its subsequent distribution as reported in [9]. Since two separate tunnel systems are considered, an alternative mitigation method is shown in the simulation model of Fig. 14. This model assumes cross-bonding the stray current collection systems, under crosstrack regeneration scenarios. Fig. 14 illustrates that the stray current collection cables (SCCCs) of each tunnel are linked by two conductors, one at either end of the tunnel.

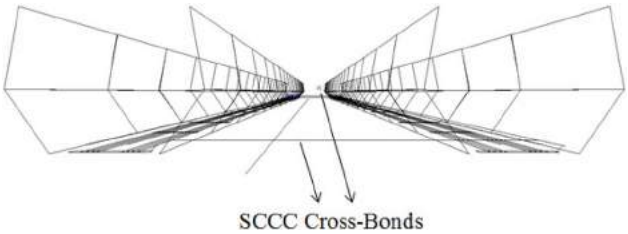

Fig. 14. Perspective view of the arrangement of conductive elements for the crosstrack regeneration model (System A—motoring at 250 m, System B—regenerating at 750 m) assuming SCCC cross-bonding at either end of the tunnels.

TABLE VI
COMPARISON UNDER SCCC CROSS-BONDING

Description	No SCCC Cross Bonding Fig. 9	SCCC Cross Bonding Fig. 14
Total Stray Current Rails	150.87 mA	150.96 mA
Retained Current S.C.C.G.	19.23 mA	59.32 mA
Retained Current S.C.C.C.	12.57 mA	52.62 mA
Total Stray Current Tunnel Services	0.00 mA	0.00 mA
Retained Current Tunnel Services	0.00 mA	0.00 mA
Retained Current 3rd party Infrastructure	0.368 mA	0.134 mA
Efficiency of S.C.C.S	21.08%	74.15 %
Current through unintended paths	78.92 %	25.85 %

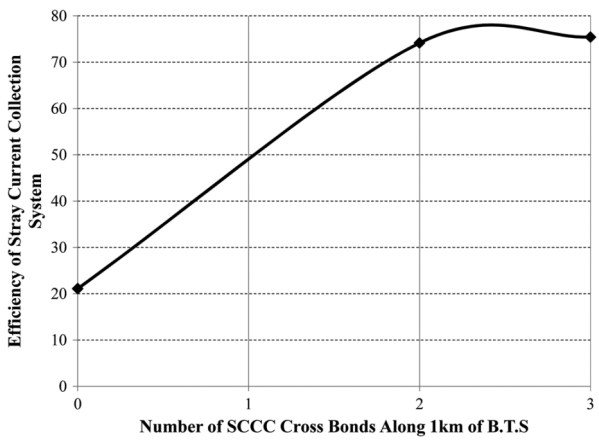

Fig. 15. Efficiency variation of stray current collection system when SCCC cross bonds are introduced along the 1 km BTS modeled.

It is noted that the model assumes the (0–100) energization scenario.

Table VI summarizes the results obtained for the model of Fig. 14 and benchmarks these against the 0–100 energization scenario results (see Table V) where no SCCC cross bonds are considered. That is to facilitate a valid comparison. Therefore, under the design inputs assumed (see Table II), the total stray current collected by the stray current collection system (SCCG + SCCC), when SCCC cross-bonding is assumed, increases by 53.07%. Consequently, less stray current flows through unintended paths to reach any third-party infrastructure in the nearby vicinity. In this particular model, the current collected by the third-party infrastructure is decreased to 0.134 mA (i.e., 63.58% reduction).

Fig. 15 illustrates the effect of introducing SCCC cross bonds at more frequent intervals along the tunnel length.

It shows the impact on the efficiency of the stray current collection system when: 1) no cross bonds are introduced; 2) two cross bonds (0–1000 m) are introduced; and 3) three cross bonds are present (0–500–1000 m). The obtained results suggest that under crosstrack regeneration scenarios, tunnel-to-tunnel cross-bonding (through SCCC) could be a valuable tool to reinstate the benefits of a stray current collection system. An important conclusion is that the use of two cross bonds at either ends of the system will suffice. The use of more SCCC cross bonds will not significantly improve the efficiency of the collection system.

IV. CONCLUSION

This paper describes a first attempt to model and quantify the effect of crosstrack regeneration on the stray current performance of a dc transit system. The cases modeled probably represent a worst case scenario but do demonstrate that regenerative braking acts to partially defeat the benefits of the stray current control system. This is unavoidable and can be minimized by maintenance of a high rail-to-earth resistance or by frequent tunnel-to-tunnel cross-bonding. Finally, the effect of regenerative braking should be kept in mind during any preliminary assessments that are performed to substantiate the design specification as well as the geometric topology of a stray current collection system.

REFERENCES

[1] P. J. Aylott, "Stray current is for life-not just for Christmas. Stray current corrosion management strategies for DC traction systems," in *Inst. Elect. Eng. Seminar DC Traction Stray Current Control—Offer a Stray a Good Ohm?*, Oct. 21, 1999, pp. 7/1–7/6.

[2] S. Case, "So what's the problem? [DC traction stray current control]," in *Inst. Elect. Eng. Seminar DC Traction Stray Current Control—Offer a Stray a Good Ohm?*, Oct. 21, 1999, pp. 1/1–1/6.

[3] L. Ardizzon, P. Pinato, and D. Zaninelli, "Electric traction and electrolytic corrosion: A software tool for stray currents calculation," in *Proc. IEEE Power Eng. Soc. Transm. Distrib. Conf. Expo.*, Sep. 7–12, 2003, vol. 2, pp. 550–555.

[4] I. Cotton, C. Charalambous, P. Ernst, and P. Aylott, "Stray current control in DC mass transit systems," *IEEE Trans. Veh. Technol.*, vol. 54, no. 2, pp. 722–730, Mar. 2005.

[5] J. G. Yu and C. J. Goodman, "Modelling of rail potential rise and leakage current in DC rail transit systems," in *Inst. Elect. Eng. Colloq. Stray Current Effects DC Railways Tramways*, Oct. 11, 1990, pp. 2/2/1–2/2/6.

[6] K. D. Pham, R. S. Thomas, and W. E. Stinger, "Analysis of stray current, track-to-earth potentials and substation negative grounding in DC traction electrification system," in *Proc. IEEE/ASME Joint Railroad Conf.*, Apr. 17–19, 2001, pp. 141–160.

[7] C.-H. Lee, "Evaluation of the maximum potential rise in taipei rail transit systems," *IEEE Trans. Power Del.*, vol. 20, no. 2, pt. 2, pp. 1379–1384, Apr. 2005.

[8] B.-Y. Ku and T. Hsu, "Computation and validation of rail-to-earth potential for diode-grounded DC traction system at Taipei Rapid Transit System," in *Proc. ASME/IEEE Joint Rail Conf.*, Apr. 8, 2004, p. 41, 46.

[9] C. A. Charalambous, I. Cotton, and P. Aylott, "A simulation tool to predict the impact of soil topologies on coupling between a light rail system and buried third party infrastructure," *IEEE Trans. Veh. Technol.*, vol. 57, no. 3, pp. 1404–1416, May 2008.

[10] C. Charalambous and I. Cotton, "Influence of soil structures on corrosion performance of floating DC transit systems," *IET Res. J.—Elect. Power Appl.*, vol. 1, no. 1, pp. 9–16, Jan. 2007.

[11] D. Paul, "DC traction power system grounding," *IEEE Trans. Ind. Appl.*, vol. 38, no. 3, pp. 818–824, May/Jun. 2002.

[12] C.-H. Lee and H.-M. Wang, "Effects of grounding schemes on rail potential and stray currents in Taipei Rail Transit Systems," *Proc. Elect. Power Appl.*, vol. 148, no. 2, pp. 148–154, Mar. 2001.

[13] R. J. Hill, Y. Cai, S. H. Case, and M. R. Irving, "Iterative techniques for the solution of complex DC-rail-traction systems including regenerative braking," *Proc. Inst. Elect. Eng., Gen., Transm. Distrib.*, vol. 143, no. 6, pp. 613–615, Nov. 1996.
[14] J. Peter Nicholson, "Correcting CIPS surveys for stray and telluric current interference," presented at the CORROSION, Nashville, TN, Mar. 11–15, 2007.
[15] M. Brenna, A. Dolara, S. ?Leva, and D. ?Zaninelli, "Effects of the DC stray currents on subway tunnel structures evaluated by FEM analysis," presented at the IEEE Power Energy Soc. Gen. Meeting, Minneapolis, MN, Jul. 25–29, 2010.
[16] A. Dolara, F. Foiadelli, and S. Leva, "Stray current effects mitigation in subway tunnels," *IEEE Trans. Power Del.,* vol. 27, no. 4, pp. 2304–2311, Oct. 2012.
[17] CDEGS Software, Safe Engineering Services & Technologies Ltd. Montreal, QC, Canada.
[18] C. A. Charalambous, I. Cotton, P. Aylott, and N. Kokkinos, "A holistic stray current assessment of bored tunnel sections of DC transit systems," *IEEE Trans. Power Del.*, vol. 28, no. 2, pp. 1048–1056, Nov. 2012.
[19] F. P. Dawalibi, J. Ma, and R. D. Southey, "Behaviour of grounding systems in multilayer soils: A parametric analysis," *IEEE Trans. Power Del.*, vol. 9, no. 1, pp. 334–342, Jan 1994.
[20] A. Ogunsola, A. Mariscotti, and L. Sandrolini, "Estimation of stray current from a DC-electrified railway and impressed potential on a buried pipe," *IEEE Trans. Power Del.*, vol. 27, no. 4, pp. 2238–2246, Oct. 2012.
[21] EN 50122-2, Railway Applications—Fixed Installations—Electrical Safety, earthing and the return circuit—Part 2: Provisions against the effect of stray currents caused by d.c. traction systems, Oct. 2010.
[22] R. G. Fletcher, "Regenerative equipment for railway rolling stock," *Power Eng. J.*, vol. 5, no. 3, pp. 105–114, May 1991.
[23] *Protection Against Corrosion by Stray Current From Direct Current Systems*, EN-50162-2004, Aug. 2004.
[24] C. A. Charalambous and I. Cotton, *Stray Current Control and Corrosion Limitation for DC Mass Transit Systems*. Manchester, U.K.: University of Manchester, 2011. [Online]. Available: https://www.escholar.manchester.ac.uk/uk-ac-man-scw:141928)

Charalambos A. Charalambous (M'13) received the Class I B.Eng. (Hons.) degree in electrical and electronic engineering and the Ph.D. degree in electrical power engineering from the University of Manchester Institute of Science and Technology, Manchester, U.K, in 2002 and 2006, respectively.

Since 2010, he has been an Assistant Professor in the Department of Electrical and Computer Engineering, University of Cyprus, Nicosia. Prior to this appointment, he was with the Electrical Energy and Power Systems Group, School of Electrical and Electronic Engineering, University of Manchester. His current research interests include power-induced corrosion, ferroresonance, and risk-management applications in power systems.

Ian Cotton (M'98–SM'07) received the Class I B.Eng. (Hons.) degree in electrical engineering from the University of Sheffield, Sheffield, U.K., in 1995 and the Ph.D. degree in electrical engineering from the University of Manchester Institute of Science and Technology, Manchester, U.K., in 1998.

Currently, he is Professor of High Voltage Technology, School of Electrical and Electronic Engineering, Electrical Energy and Power Systems Group, University of Manchester, Manchester, U.K. His current research interests include power systems transients, the use of higher voltage systems in aerospace applications, and power system-induced corrosion.

Prof. Cotton is a Chartered Engineer.

Pete Aylott received the M.A. degree (Hons.) in natural sciences from the University of Cambridge, Cambridge, U.K., in 1981.

Since 1985, he has been with CAPCIS Ltd. (now Intertek-CAPCIS), Manchester, U.K., where he is currently the Commercial Director. His consultancy experience covers the management of stray current on light rail and heavy rail underground systems and the interactions between these and the utility systems both across the U.K. and overseas.